Journal of Neuroinflammation

RESEARCH Open Access

Probiotics alleviate painful diabetic neuropathy by modulating the microbiota–gut–nerve axis in rats

Ye Jiang[1†], Jing Yang[1†], Min Wei[1], Jiayin Shou[1], Shixiong Shen[1], Zhuoying Yu[1], Zixian Zhang[2,3,4], Jie Cai[2,3,4], Yanhan Lyu[1], Dongsheng Yang[1], Yongzheng Han[1], Jinpiao Zhu[5], Zhigang Liu[5], Daqing Ma[5,6*], Guo-gang Xing[2,3,4*] and Min Li[1*]

Abstract
Painful diabetic neuropathy (PDN) is one of the most common complications of diabetes. Recent studies suggested that gut microbiota dysbiosis contributes to the development of PDN, but underlying mechanisms remain elusive. In this study, we found decreased probiotics generating bacteria such as *Lactobacillus* and *Bifidobacterium* strains in the PDN rats. Supplementation with multiple probiotics for 12 weeks alleviated pain, reversed nerve fiber lesions, and restored neuronal hyperexcitability. Probiotics administration effectively attenuated intestinal barrier impairment, reduced serum lipopolysaccharide and proinflammatory cytokines, and mitigated disruptions in the blood-nerve barrier. Furthermore, probiotics treatment inhibited the activation of the TLR4/MyD88/NF-κB signaling pathway and reduced proinflammatory cytokines in the sciatic nerve of the PDN rats. Together, our findings suggest that gut microbiota dysbiosis participates in PDN pathogenesis, and probiotics offer therapeutic potential *via* modulating the microbiota-gut-nerve axis.

Introduction

The prevalence of type 2 diabetes (T2D) is rising worldwide [1]. Neuropathy is one of the most common complications of diabetes, with approximately one in five diabetic patients suffering from painful diabetic neuropathy (PDN) [2]. The symptoms of PDN severely impact patients' quality of life [3]. The pathogenesis of PDN is complicated with involvements of neuroinflammation, oxidative stress, mitochondrial dysfunction, and cell death as well as microangiopathy [4]. Current therapies for PDN remain limited, primarily focusing on glycemic control and symptomatic treatment [4]. Only a third of patients achieve 50% pain relief, often accompanied by troublesome side effects and low satisfaction [5]. Therefore, it is urgent to investigate PDN pathogenesis and its underlying mechanisms and to develop new treatment strategies.

The gut microbiota plays crucial roles in various aspects of host health, including digestion, metabolism, immune function, and neurological processes [6]. Imbalance of gut microbiota (dysbiosis) is associated with various chronic diseases, including inflammatory bowel diseases, obesity, diabetes, autoimmune disorders, and mental health problems such as depression and anxiety

[†]Ye Jiang and Jing Yang contributed equally to this work.

*Correspondence:
Daqing Ma
d.ma@imperial.ac.uk; daqingma91@zju.edu.cn
Guo-gang Xing
ggxing@bjmu.edu.cn
Min Li
liminanesth@bjmu.edu.cn

Full list of author information is available at the end of the article

Graphical abstract

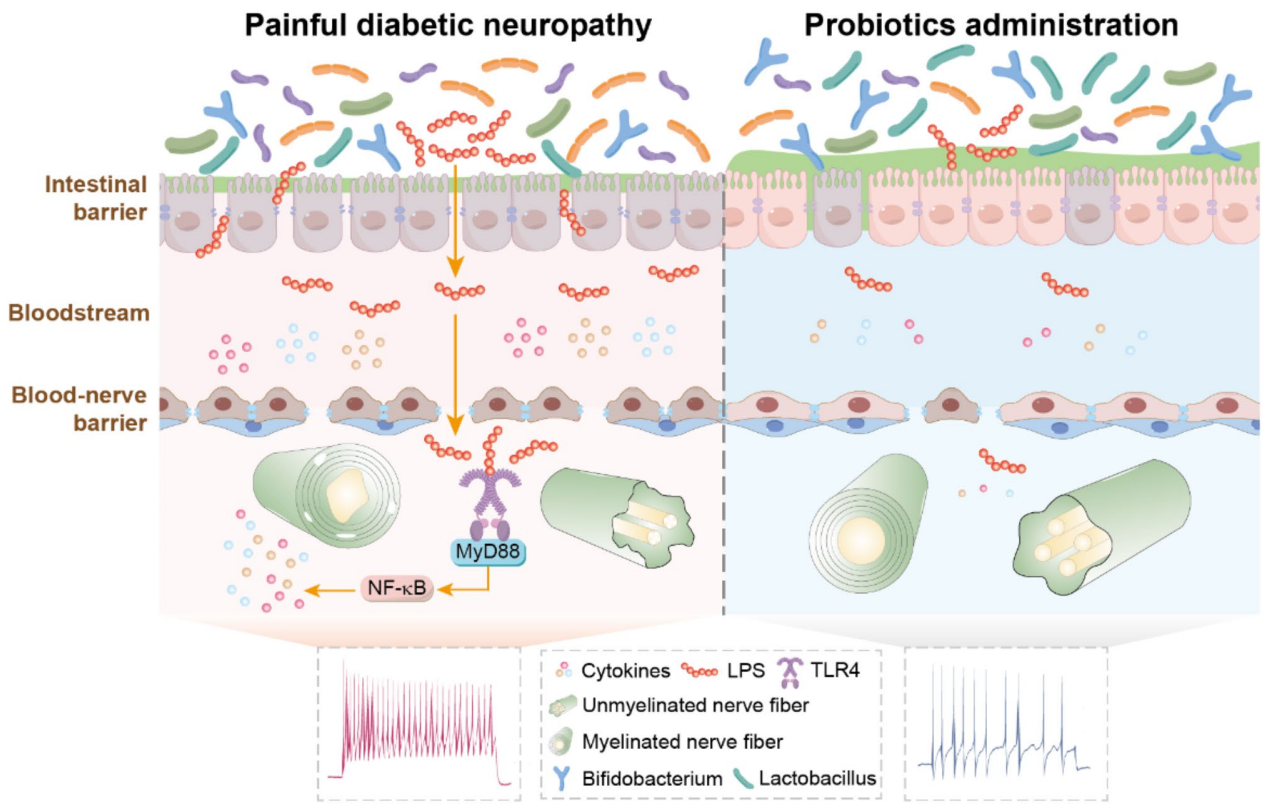

Keywords Painful diabetic neuropathy, Microbiota–gut–nerve axis, Probiotics, Neuroinflammation

[7]. A very recent study with a small sample size showed that PDN patients exhibit a distinct microbiota signature *versus* healthy controls, with a significant decrease in the richness of *Bacteroides* and *Faecalibacterium* at the genus level, and an increase in *Escherichia-Shigella*, *Lachnoclostridium*, *Blautia*, *Megasphaera*, and *Ruminococcus torques* [8]. Another elegant study even classified gut microbiota in PDN patients into two competing ecological groups (guilds): Guild 1, which is potentially beneficial with higher genetic capacity for butyrate production and fewer endotoxin synthesis genes, and Guild 2, which is potentially harmful. And dysbiosis in PDN patients was characterized by a decrease in Guild 1 and an increase in Guild 2. Moreover, gut microbiota from PDN patients worsen peripheral neuropathy in T2D mice [9]. Cumulatively, these findings suggested that gut microbiota dysbiosis may contribute to the development of PDN. However, further investigation is needed to elucidate underlying mechanisms.

Abnormalities in the gut microbiota contributed to disrupted intestinal barrier and elevated gut permeability in obesity and T2D in disease models and patients [10, 11]. Consequently, the compromised intestinal barrier allows the entry of gut microbiota-derived molecules like lipopolysaccharide (LPS) into the bloodstream, which in turn promotes systemic inflammation in metabolic disorders [12].

The systemic inflammation caused by gut dysbiosis triggers the disruption of the blood-brain barrier (BBB) and contributes to pathogenesis of neurodegenerative disorders, such as Alzheimer's disease [13], Parkinson's disease [14], and multiple sclerosis [15]. This disruption facilitates the passage of proinflammatory factors into the brain, leading to neuroinflammation. Considering that the blood-nerve barrier (BNB) shares a similar structure to the BBB, which prevents the entry of harmful molecules into neural tissues, it is hypothesized that gut dysbiosis-induced metabolic inflammation in T2D may also disrupt the BNB and induce peripheral neuroinflammation and injury.

Microbiota-targeted interventions, such as fecal microbiota transplantation (FMT), probiotics, prebiotics, and dietary management, were reported to have the potential to optimize the composition and function of the gut microbiota for disease treatment [6]. Indeed, probiotic intervention reshapes the composition and structure of

gut microbiota, thereby improving glycemic control and enhancing insulin sensitivity in diabetic mice [11]. Moreover, further preclinical and clinical studies demonstrated that probiotics have potential therapeutic effects in diabetic complications, such as diabetic nephropathy, retinopathy, neuropathy, and cerebrovascular disease [11].

Accordingly, we, therefore, hypothesized that gut dysbiosis may compromise both the intestinal barrier and BNB, triggering systemic inflammation and subsequent neuroinflammation towards PDN development, and administering probiotics may offer therapeutic benefits for PDN by modulating gut dysbiosis. In this study, we used a well-established PDN rat model to explore these hypotheses and underlying mechanisms.

Methods

Animals

All animal experiments in this study were approved by the Peking University Animal Care and Use Committee (approval no. LA2023082) and followed the ARRIVE guideline. Healthy male Sprague-Dawley rats (160-200 g, 6-8 weeks) were purchased from the Department of Experimental Animal Sciences, Peking University Health Science Center, Beijing, China. They were housed at standard conditions (temperature 24 ± 1 ℃ and humidity 50-60% on a 12/12 h light/dark cycle) with free access to food and water.

Experimental design

Experiment I: T2D model induction

After one week of acclimatization, rats were randomly divided into two groups. The control group was given a normal chow diet, while the PDN group was fed a high-fat diet (HFD, Research Diets, catalog D12451). The normal chow diet comprised 11.5% fat, 20.8% protein, and 67.7% carbohydrate, while the HFD consisted of 45% fat, 20% protein, and 35% carbohydrate. After 8 weeks, the rats in the PDN group were fasted for 12 h and then injected intraperitoneally with streptozotocin (STZ, Sigma-Aldrich) at a dose of 30 mg/kg. The control group rats were injected with a vehicle containing an equivalent amount of sodium citrate-citric acid buffer. Fasting blood glucose levels ≥ 11.1 mmol/L on day 3 post-injection were considered to be T2D rats. An intraperitoneal glucose tolerance test (IPGTT) was performed following a 12-hour fast on day 7 after the STZ injection. A 50% glucose solution (2 g/kg) was administered intraperitoneally, and the blood glucose levels were monitored before and after injection at 30, 60, 90, and 120 min, respectively, to confirm the model's success for further experiment use. The T2D rats were fed HFD until the end of the study.

Experiment II: administration of probiotics

According to previous studies [16], supplementing with multiple probiotic strains or high-dose supplements may be superior to single strains or low doses. Therefore, we selected a multi-strain probiotic supplementation strategy that incorporates bacteria downregulated in the PDN group. Concurrently fed with the HFD, rats were divided into two groups supplemented with or without compound probiotics by daily intragastric gavage for 12 weeks. Rats in the probiotics group received 24×10^9 colony-forming units (CFU)/day of probiotics dissolved in phosphate-buffered saline (PBS), while rats in the other groups received equal volumes of PBS. The dosage of the compound probiotics (24×10^9 CFU/day) was referred to the previous studies [17–19] that demonstrated beneficial effects on anti-inflammatory responses or neuroprotection. The compound probiotics were purchased from Life Space Co., Ltd. (Australia), containing nine *Lactobacillus* species (*L. rhamnosus*, *L. plantarum*, *L. rhamnosus GG*, *L. casei*, *L. paracasei*, *L. rhamnosus*, *L. gasseri*, *L. delbrueckii ssp. Bulgaricus*, and *L. reuteri 1E1*), five *Bifidobacterium* species (*B. lactis*, *B. animalis ssp. lactis*, *B. breve*, *B. longum*, and *B. infantis*), and *Streptococcus thermophilus*.

Behavioral tests

After STZ injection, rats were assessed pain threshold once a week until sacrifice. All animals were placed in a clear plastic container and allowed to acclimate for a minimum of 30 min before testing. All behavioral experiments were conducted in a blinded manner.

Mechanical allodynia

Mechanical allodynia was assessed using Von Frey according to a previous study [20].

Different intensities of von Frey fibers were applied to the mid-plantar surface of the hind paw in an alternating manner. The "up and down" method was used to determine mechanical sensitivity with a 50% likelihood of paw withdrawal threshold (PWT).

Thermal hyperalgesia

Accordingly [21], thermal hyperalgesia was tested with a Hargreaves apparatus. A radiant heat source was directed towards the plantar surface of the hind paw. To measure the paw withdrawal latency (PWL), a timer was started when the heat source was activated and stopped when paw withdrawal was detected. Each paw was tested three times with at least a five-minute gap between each test.

Measurement of the sensory nerve conduction velocity (SNCV)

At week 4 post-STZ injection, SNCV was measured using a previously described noninvasive procedure in

the digital nerve [22], with the results reported in meters per second.

Acute dissociation of dorsal root ganglion (DRG) neurons and whole-cell patch-clamp recordings

As previously described [20], L4 and L5 DRGs were collected and digested at week 4 following STZ injection. The dissociated small neuronal cells were then used for patch-clamp recording. Data analysis was carried out using Origin software 9.0 (OriginLab Corporation, Northampton, MA).

Assessment of BNB function

BNB permeability was evaluated following previously established methods [23, 24]. At week 4 following STZ injection, anesthetized rats received intravenous injections by the tail vein of either 2% NaFlu (10%, 2 ml/kg, Sigma-Aldrich) or 1% EBA (5% bovine albumin labeled with 1% Evans blue, 10 ml/kg, Sigma-Aldrich). After 30 min of circulation, their sciatic nerves were harvested after perfusion, fixed in 4% paraformaldehyde (PFA) for 1 h, and embedded in the Tissue-Tek O.C.T. compound. Sciatic nerve sections with a thickness of 10 μm were obtained and examined by fluorescence microscopy.

Tissue and blood collection

At week 4 following STZ injection and behavioral assessments, rats were anesthetized, and blood was collected. They were then perfused transcardially with saline to remove residual blood. Sciatic nerves and colons were carefully dissected and harvested. The tissues of sciatic nerves and colons were divided: portions were snap-frozen in liquid nitrogen for western blot (WB) or fixed in 4% PFA for immunofluorescence staining and hematoxylin and eosin (H&E) staining. Additionally, some portions of sciatic nerves were fixed in 3% glutaraldehyde for transmission electron microscopy (TEM).

Transmission Electron Microscope (TEM)

As previously described [25], the sciatic nerve was immersed in 3% glutaraldehyde at 4 ℃ for 24 h, followed by treatment with 1% osmic acid for 2 h at room temperature. After dehydration using a gradient of acetone, the tissue was embedded in epoxy and cut into ultrathin sections (70-80 nm) using an ultramicrotome. Images were acquired with a transmission electron microscope (JEOL JEM-1400).

Immunofluorescence staining

The sciatic nerve and colon were fixed in 4% PFA at 4 ℃ for 24 h. After dehydration with gradient sucrose, the tissue was embedded in Tissue Tek O.C.T. Compound and sectioned into 10 μm. For immunofluorescence staining, slices were permeabilized with 0.3% Triton X-100 in PBS and blocked with 3% bovine serum albumin. Afterward, the sections were incubated overnight at 4 ℃ with the primary antibody, rabbit anti-zonula occludens-1 (ZO-1, 1:100, ab221547; Abcam). Following PBS washing, the samples were then treated with the secondary antibody, goat anti-rabbit IgG Alexa Fluor® 594 (1:500, ZF-0516; ZSGB-BIO). Nuclei were stained with DAPI solution (2 μg/mL). The stainings were observed through fluorescent microscopy using the same settings for each antibody. The positive area was quantified using Image Pro Plus 6.0 software.

H&E staining

Colon tissues were fixed in 4% PFA overnight and embedded in paraffin. H&E staining was performed as previously described [26].

Enzyme-Linked Immunosorbent Assay (ELISA)

Serum levels of interleukin-6 (IL-6), interleukin-1β (IL-1β), and tumor necrosis factor-α (TNF-α) were measured using the ELISA kits (Dakewe Bioengineering, Shenzhen, China), and the LPS and LPS binding protein (LBP) measured with ELISA kits (Jianglai Industrial Limited By Share Ltd, Shanghai, China).

Western blot

The sciatic nerve and colon tissues were lysed in RIPA lysis buffer (C1055, APPLYGEN, China) with proteinase inhibitor (K1007, Apexbio, USA) and phosphate inhibitor (P1265, APPLYGEN, China). Protein content was analyzed using the bicinchoninic acid Protein Assay Kit (P1511, APPLYGEN, China). The protein samples were separated using sodium dodecyl sulfate polyacrylamide gel electrophoresis, transferred to polyvinylidene fluoride membranes (Merk Millipore), and blocked with 5% fat-free milk for 60 min. The blots were incubated with the following primary antibodies: rabbit anti-ZO-1 (1:1000, 61-7300; Thermo Fisher Scientific), mouse anti-occludin (1:1000, 33-1500; Thermo Fisher Scientific), rabbit anti-claudin-1 (1:2000, T56872; Abmart), mouse anti-claudin-5 (1:1000, 35-2500; Thermo Fisher Scientific), mouse anti-toll-like receptor 4 (TLR4, 1:1000, 66350-1-Ig; Proteintech), mouse anti-myeloid differentiation factor 88 (MyD88, 1:1000, 67969-1-Ig; Proteintech), rabbit anti-inhibitor of κBα (IκBα, 1:1000, T55026; Abmart), rabbit anti-phosphorylated-IκBα (1:1000, T56280; Abmart), rabbit anti-nuclear factor-κB p65 (NF-κB p65, 1:5000, T55034; Abmart), and rabbit anti-phosphorylated-NF-κB p65 (p-p65, 1:2000, 82335-1-RR; Proteintech). Following incubation with HRP-conjugated secondary antibodies (ZSBIO), enhanced chemiluminescent agent (Applygen) was used to detect the signal. Images were captured on a Tanon chemiluminescence system. Band density was determined using ImageJ software.

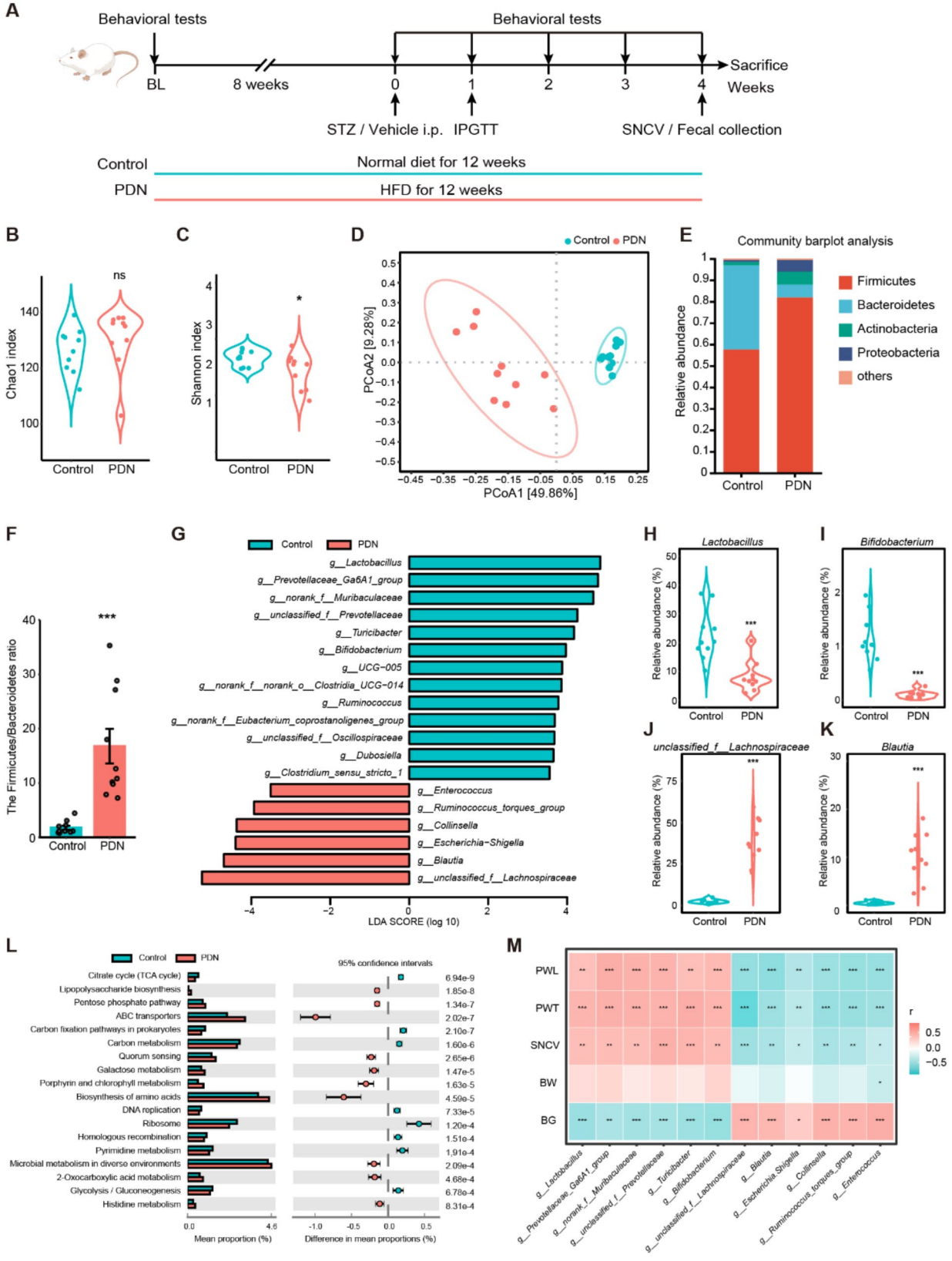

Fig. 1 (See legend on next page.)

(See figure on previous page.)

Fig. 1 Gut microbiota dysbiosis in the PDN rats. (**A**) Flowchart of the Experiments I. (**B, C**) Alpha-diversity measured by Chao1 and Shannon index. (**D**) Principal coordinate analysis (PCoA) plot of Bray-Curtis dissimilarity at the ASV level. (**E**) Relative abundance of gut microbiota at the phylum level. (**F**) The Firmicutes/Bacteroidetes ratio. (**G**) Bar graph of the different abundant taxa based on the cutoff value of LDA score (log10) > 3.5 and $P < 0.05$. (**H-K**) Relative abundance of representative bacterial genera: *Lactobacillus*, *Bifidobacterium*, *unclassified_f__Lachnospiraceae,* and *Blautia*. (**L**) Pathway enrichment analysis of significantly altered KEGG pathways. (**M**) Spearman's correlation heatmap of gut microbial genus relative abundance with metabolic and pain-related phenotypes. PWT, paw withdrawal threshold; PWL: Paw withdrawal latency; SNCV: Sensory nerve conduction velocity; BW: Body weight; BG: Blood glucose. $n = 10$ for each group. Data are presented as mean ± SEM. $^{*}P < 0.05$, $^{**}P < 0.01$, $^{***}P < 0.001$, Mann-Whitney U test for (**B**), Student's *t*-test for (**C**), (**F**), (**H-K**), PERMANOVA for (**D**)

Gut microbiota analysis

Fecal pellets were collected, frozen in liquid nitrogen, and stored at -80 ℃ until use. The gut microbiota was analyzed using 16S rRNA sequencing.

Total genomic DNA was extracted using the PF Mag-Bind Stool DNA Kit (Omega Bio-tek, GA, USA) following the manufacturer's instructions. DNA quality and concentration were evaluated using 1.0% agarose gel electrophoresis and a NanoDrop® ND-2000 spectrophotometer (Thermo Scientific Inc., USA). The V3-V4 region of bacterial 16S rRNA genes was amplified with primer pairs 338 F and 806R using an ABI GeneAmp® 9700 PCR thermocycler. PCR conditions included an initial denaturation at 95 ℃ for 3 min, followed by 27 cycles of denaturation at 95 ℃ for 30 s, annealing at 55 ℃ for 30 s, extension at 72 ℃ for 45 s, and a final extension at 72 ℃ for 10 min. PCR products were purified and quantified before being pooled equimolarly and sequenced on an Illumina PE300 platform.

The resulting sequences were quality-checked using fastp (version 0.19.6) [27] and merged with FLASH (version 1.2.11) after demultiplexing. High-quality sequences were denoised using the DADA2 plugin in the Qiime2 (version 2020.2) pipeline to obtain amplicon sequence variants (ASV). Taxonomic assignment of ASV was performed using the Naïve Bayes consensus taxonomy classifier implemented in QIIME2 along with the SILVA 16 S rRNA database (version 138).

Alpha diversity indices including Chao1 richness and Shannon index were calculated using Mothur (version 1.30.2). The similarity among microbial communities in different samples was assessed by principal component analysis (PCA) or principal coordinate analysis (PCoA) based on Bray-Curtis dissimilarity using the Vegan (version 2.4.3) package. The linear discriminant analysis (LDA) effect size (LEfSe) (http://huttenhower.sph.harvard.edu/LEfSe) was performed to identify the significantly abundant taxa of bacteria among the different groups. Functional prediction was analyzed using PICRUSt2 (Phylogenetic Investigation of Communities by Reconstruction of Unobserved States) to identify the enrichment of Kyoto Encyclopedia of Genes and Genomes (KEGG) pathways. Spearman's correlations were calculated to assess the association between the differing abundances of PDN-associated genus and metabolic status as well as pain. The correlation heatmaps were generated in R (v4.3.2).

Serum Short Chain Fatty Acids (SCFAs)

Serum SCFAs were analyzed using gas chromatography-tandem mass spectrometry (GC-MS/MS). Briefly, 50 µL of serum was mixed with 100 µL of 0.5% (v/v) phosphoric acid and vortexed for 3 min. Then, 150 µL of MTBE containing an internal standard was added, followed by another vortex for 3 min and a 5-minute ultrasonication. The mixture was centrifuged at 12,000 r/min for 10 min at 4°C. An Agilent 7890B gas chromatograph coupled to a 7000D mass spectrometer, equipped with a DB-FFAP column, was used for SCFA detection.

Statistical analysis

Data were presented as mean ± standard error of mean (SEM) and analyzed using GraphPad Prism 9 (GraphPad Software, La Jolla, CA). Normality tests were conducted using the Shapiro-Wilk tests, and a Mann-Whitney U or Kruskal Wallis test was applied to data that did not pass the test for normality. If normally distributed, the two-tailed, unpaired Student's *t*-test was used for comparing two groups, while one- or two-way ANOVA with Sidak's or Tukey's multiple comparisons test was applied to compare multiple groups, as appropriate. We used PERMANOVA (permutational multivariate analysis of variance) to test for significant differences in microbial community structure. A *P* value less than 0.05 was considered to be statistically significant.

Results

Gut microbiota dysbiosis

An 8-week HFD followed by STZ injection was used to induce T2D rats (Fig. 1A), resulting in gradual weight loss (group: $F_{(1, 18)} = 21.55$, $P < 0.0001$; week: $F_{(1.982, 35.67)} = 1546$, $P < 0.0001$; interaction: $F_{(5, 90)} = 84.83$, $P < 0.0001$, Figure S1A), blood glucose increase (group: $F_{(1, 18)} = 551.8$, $P < 0.0001$; week: $F_{(3.204, 57.68)} = 126.3$, $P < 0.0001$; interaction: $F_{(5, 90)} = 123.9$, $P < 0.0001$, Figure S1B), and glucose intolerance (group: $F_{(2, 27)} = 10.14$, $P < 0.0001$; time: $F_{(1.735, 46.83)} = 41.03$, $P < 0.0001$; interaction: $F_{(16, 216)} = 9.694$, $P < 0.0001$, Figure S1C). The corresponding area under the curve (AUC) of IPGTT was increased ($t = 21.54$, df = 18, $P < 0.0001$, Figure S1D). After STZ injection, the T2D rats exhibited a decreased SNCV ($t = 6.163$, df = 18,

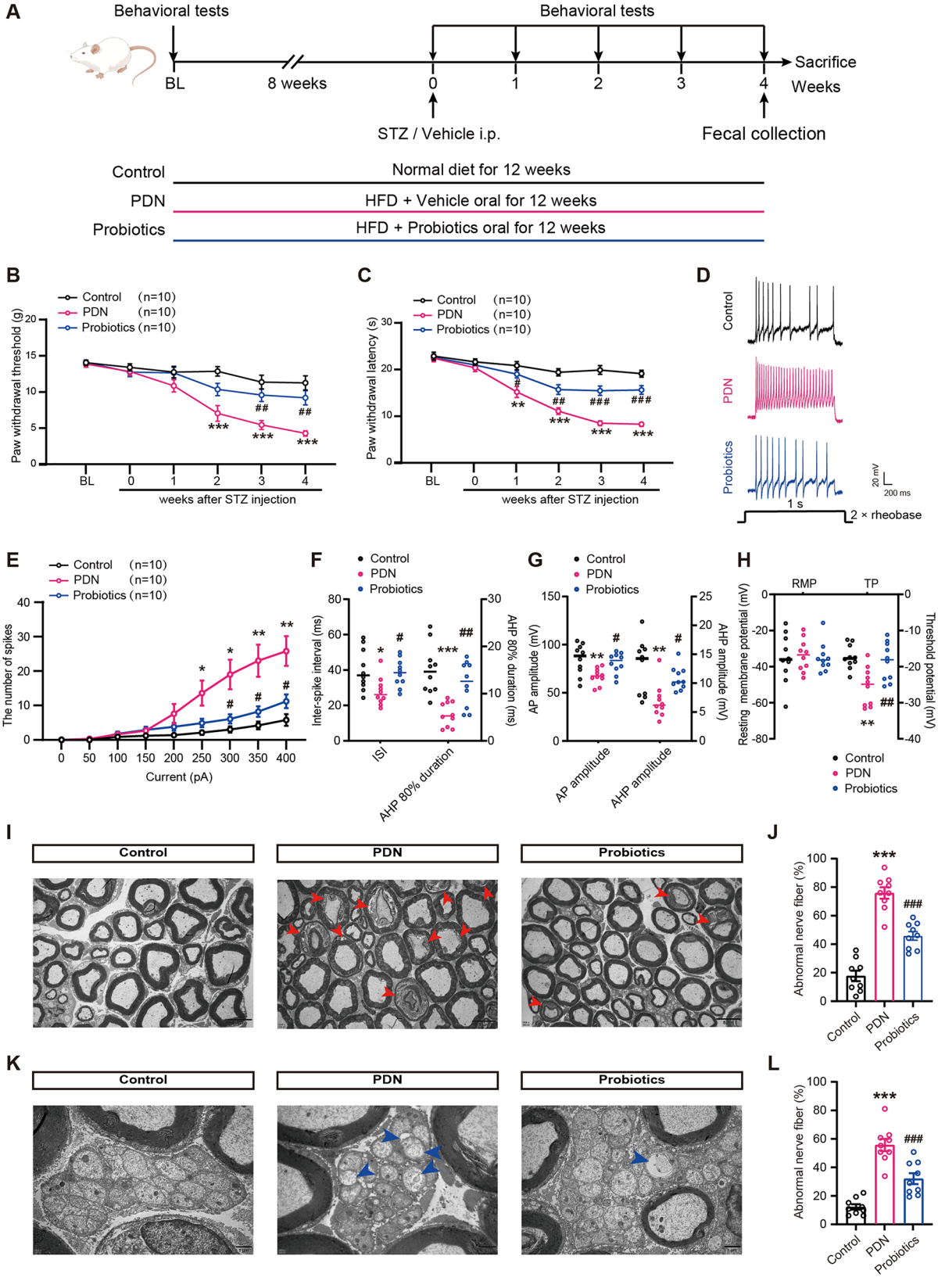

Fig. 2 (See legend on next page.)

(See figure on previous page.)

Fig. 2 Probiotics treatment reduced pain and nerve damage in PDN rats. (**A**) Flowchart of the experiments. Vehicle: citric acid-sodium citrate buffer. (**B, C**) The test of mechanical allodynia and thermal hyperalgesia from baseline (BL) to week 4 following streptozotocin (STZ) injection ($n = 10$). (**D-H**) showed the results of single-cell patch clamp recordings at week 4 after STZ injection. (**D**) Representative traces of neuronal action potential (AP). (**E-H**) Statistical analysis of the AP number, inter-spike interval (ISI), after-hyperpolarization (AHP) duration at 80% recovery time (AHP 80% duration), AP amplitude, resting Membrane Potential (RMP), and threshold potential (TP) in DRG neurons of PDN rats ($n = 3$). (**I**) Representative electron micrographs of myelinated axons in the sciatic nerve. The panel represents 1000× magnified images (scale bar = 5 μm). The red arrows indicate a damaged myelinated sheaths (myelin sheath fragment, and lamellar separation) ($n = 3$ fields of view for each group of three rats). (**J**) Statistical analysis of the proportion of abnormal myelinated fibers relative to the total number of myelinated fibers. (**K**) Representative electron micrographs of unmyelinated axons in the sciatic nerve. The panel represents 4000× magnified images (scale bar = 1 μm). The blue arrows indicate a damaged unmyelinated axon (vacuolization) ($n = 3$ fields of view for each group of three rats). (**L**) Statistical analysis of the proportion of abnormal unmyelinated fibers relative to the total number of unmyelinated fibers. Data are presented as mean ± SEM. $^{*}P < 0.05$, $^{**}P < 0.01$, $^{***}P < 0.001$ *versus* the control group; $^{\#}P < 0.05$, $^{\#\#}P < 0.01$, $^{\#\#\#}P < 0.001$ *versus* the PDN group, one-way ANOVA with Tukey's multiple comparisons test for (**F-H**); two-way ANOVA with Sidak's multiple comparisons test for (**B**), (**C**), and (**E**)

$P < 0.0001$, Figure S1E), mechanical allodynia (group: $F_{(1,\ 18)} = 62.87$, $P < 0.0001$; week: $F_{(3.735,\ 67.23)} = 38.45$, $P < 0.0001$; interaction: $F_{(5,\ 90)} = 34.66$, $P < 0.0001$, Figure S1F) and thermal hyperalgesia (group: $F_{(1,\ 18)} = 71.27$, $P < 0.0001$; week: $F_{(3.434,\ 61.81)} = 70.25$, $P < 0.0001$; interaction: $F_{(5,\ 90)} = 51.72$, $P < 0.0001$, Figure S1G), indicating successful modeling of PDN.

Emerging evidence suggests that gut microbiota plays a crucial role in the development of neuropathic pain [28]. Thus, we collected fecal samples for microbiota analysis. To evaluate the alterations in microbial community compositions following PDN modeling, we analyzed the alpha and beta diversity in the PDN rats compared to the controls. In alpha diversity, no difference was observed in the Chao1 index (Mann-Whitney U test, 130.60 ± 3.42 vs. 126.50 ± 2.51, U = 31.50, $P = 0.1712$, Fig. 1B), while the Shannon index was higher in the PDN group than the control group (2.43 ± 0.10 vs. 2.67 ± 0.04, $t = 2.199$, df = 18, $P = 0.0412$, Fig. 1C). Beta diversity analysis using principal coordinate analysis (PCoA) at the amplicon sequence variants (ASV) level revealed significant clustering differences in microbial community structure between the two groups ($P < 0.0010$, Fig. 1D).

To further explore the alterations in microbiota structure between the two groups, relative abundance at the phylum and genus levels was found. At the phylum level, Firmicutes and Bacteroidetes were predominant in both groups (Fig. 1E), with the PDN group exhibiting a higher Firmicutes/Bacteroidetes (F/B) ratio compared to the controls (16.78 ± 3.18 vs. 1.79 ± 0.38, $t = 2.199$, df = 18, $P = 0.0002$, Fig. 1F). Next, we determined the percentage of bacterial taxa and conducted linear discriminant analysis (LDA) effect size (LEfSe) to identify genomic traits of the gut microbiota (Fig. 1G). At the genus level, the PDN rats exhibited a reduction in *Lactobacillus* (8.10 ± 1.64 vs. 22.48 ± 2.74, $t = 4.497$, df = 18, $P = 0.0003$, Fig. 1H) and *Bifidobacterium* (0.10 ± 0.02 vs. 1.15 ± 0.14, $t = 7.586$, df = 18, $P < 0.0001$, Fig. 1I), both widely recognized as probiotics and associated with the production of short chain fatty acids (SCFAs) [29]. Conversely, the abundance of *unclassified_f__Lachnospiraceae* (38.35 ± 4.18 vs. 2.54 ± 0.33, $t = 8.535$, df = 18, $P < 0.0001$, Fig. 1J) and *Blautia* (10.26 ± 1.56 vs. 0.55 ± 0.09, $t = 6.228$, df = 18, $P < 0.0001$, Fig. 1K) was significantly higher in the PDN group.

To better understand the function of these significantly altered bacteria, we performed a functional analysis of KEGG pathway enrichment. A total of 18 KEGG pathways at the level 3 was identified (Fig. 1L). The PDN group showed a marked increase in functions related to lipopolysaccharide biosynthesis, pentose phosphate pathway, ATP-binding cassette (ABC) transporters, quorum sensing, galactose metabolism, porphyrin, and chlorophyll metabolism, biosynthesis of amino acids, microbial metabolism in diverse environments, and 2-Oxocarboxylic acid metabolism.

To correlate the relative abundance of microbiota associated with PDN features, we performed a correlation analysis of the differential genera to metabolic and PDN phenotyping at week 4 post-STZ injection (Fig. 1M). We found some genera, such as *Lactobacillus and Bifidobacterium*, had a positive correlation to pain threshold and SNCV.

To investigate alterations in microbiota-derived metabolites, we focused on short-chain fatty acids (SCFAs), which are linked to metabolic and neurological diseases [30]. While most SCFAs showed no significant differences between groups (Figure S2A), serum propionate levels were notably higher in the PDN group compared to controls (0.13 ± 0.02 vs. 0.18 ± 0.02, $t = 2.136$, df = 17, $P = 0.0475$, Figure S2B).

Probiotics treatment reduced pain and nerve damage

Based on the correlation between the decreased levels of *Lactobacillus and Bifidobacterium* genera and lower pain thresholds observed in the PDN rats, we conducted a 12-week targeted supplementation of the deficient probiotics in the PDN rats to investigate the potential of these probiotics in alleviating pain (Fig. 2A). HFD and STZ injection induced mechanical allodynia and thermal hypersensitivity indicated by a significant reduction of the PWT (group: $F_{(2,\ 27)} = 12.77$, $P < 0.0001$; week: $F_{(3.302,\ 89.16)} = 48.88$, $P < 0.0001$; interaction: $F_{(10,\ 135)} = 7.188$, $P < 0.0001$, Fig. 2B) and PWL (group: $F_{(2,\ 27)} = 60.52$,

$P < 0.0001$; week: $F_{(4.195,\ 113.3)} = 62.22$, $P < 0.0001$; interaction: $F_{(10,\ 135)} = 9.670$, $P < 0.0001$, Fig. 2C) in the PDN rats versus controls from week 2 post-STZ injection. The rats in the probiotics group exhibited higher PWT at week 3 and 4 post-STZ injection (Fig. 2B), and increased PWL at week 2, 3, and 4 post-STZ injection compared to PDN rats (Fig. 2C), suggesting that probiotics alleviated both mechanical and thermal pain. Furthermore, probiotics administration mitigated neuronal hyperexcitability (Fig. 2D), shown as a significant decrease in the number of action potential (AP) (Fig. 2E), an increase in the interspike interval (ISI) ($F_{(2,27)} = 5.065$, $P = 0.0136$, Fig. 2F), after-hyperpolarization (AHP) duration at 80% recovery time (AHP 80% duration) ($F_{(2,27)} = 11.95$, $P = 0.0002$, Fig. 2F), AP amplitude ($F_{(2,27)} = 5.644$, $P = 0.0090$, Fig. 2G), AHP amplitude ($F_{(2,27)} = 7.520$, $P = 0.0025$, Fig. 2G), and threshold potential (TP) ($F_{(2,27)} = 8.734$, $P = 0.0012$, Fig. 2H). After 8 weeks on an HFD, the probiotics treatment significantly lowered body weight when compared to the PDN group, and this trend continued after STZ injection (Figure S3A). A notable difference in blood glucose was observed only at week 4 post-STZ injection (Probiotics vs. PDN, 22.38 ± 0.80 vs. 26.68 ± 1.05, $P = 0.0122$, Figure S3B).

Next, we used TEM to examine the ultrastructure of the sciatic nerve. In the PDN rats, the sciatic nerve displayed decompacted myelin sheaths with electron-sparse patches between them, along with vacuolization of unmyelinated fibers, in contrast to the intact and densely packed nerve fibers in the controls. The administration of probiotics alleviated nerve damage compared to the PDN group (Fig. 2I-L).

To observe the changes in gut microbiota after probiotic supplementation, we used 16S rRNA sequencing to analyze the gut microbiota of the PDN group and the probiotics group. The Microbial Dysbiosis Index (MDI) is an index used to determine the degree of microbial ecological imbalance, with higher values indicating greater dysbiosis. Following probiotics supplementation, the MDI significantly decreased (Mann-Whitney U test, 1.06 ± 0.18 vs. -0.94 ± 0.20, $U = 0$, $P < 0.0001$, Figure S4A). Regarding beta diversity, both PCA and PCoA analyses revealed significant differences in microbial community structure between the two groups (Figure S4B and S4C). At the phylum level, the probiotics group exhibited a reduction in Firmicutes and Proteobacteria, alongside an increase in Actinobacteria compared to the PDN group (Figure S4D). At the genus level, the probiotics group exhibited higher abundances of *Lactobacillus and Bifidobacterium*, while *Duncaniella*, *Romboutsia*, *norank_f__Porphyromonadaceae,* and *Blautia* were significantly reduced compared to the PDN group (Figure S4E). Similarly, at the species level, the probiotics group demonstrated increased levels of *Bifidobacterium_pseudolongum*, *Lactobacillus_murinus*, *Lactobacillus_johnsonii*, and *Lactobacillus_reuteri*, while *Porphyromonadaceae_bacterium_UBA7139*, *Duncaniella_dubosii*, and *Romboutsia_ilealis* were reduced compared to the PDN group (Figure S4F). Further analysis using Linear Discriminant Analysis Effect Size (LEfSe) identified species enrichment variations between the two groups, with significant enrichment observed in *Bifidobacterium_pseudolongum*, *Lactobacillus_murinus*, and *Lactobacillus_reuteri* in probiotics group (Figure S4G). Additionally, KEGG functional analysis indicated that the PDN group had enriched lipopolysaccharide biosynthesis pathways (Figure S4H).

These findings suggested that PDN rats experienced mechanical allodynia, thermal hyperalgesia, neuronal hyperexcitability, and nerve damage. Probiotics mitigated pain, nerve lesions, and microbial dysbiosis, indicating their therapeutic potential.

Probiotics treatment alleviated BNB impairment

The integrity of the BNB is essential for maintaining normal peripheral nerve function [31]. Following intravenous injection with either a low-molecular-weight tracer, NaFlu, or a high-molecular-weight tracer, EBA, BNB permeability was analyzed. A notable increase in the NaFlu fluorescence was detected in the PDN group, which was reversed by probiotics treatment ($F_{(2,6)} = 22.16$, $P = 0.0017$, Fig. 3A and B). The EBA was restricted from the inner spaces of the sciatic nerve in all three groups ($F_{(2,6)} = 2.293$, $P = 0.1820$, Fig. 3C and D).

The tight junctions play a crucial role in preserving the integrity of the BNB [32]. As shown in Fig. 3E-H, western blot analysis of sciatic nerves revealed a significant decrease of the tight junction proteins (ZO-1, occludin, and claudin-5) in the PDN group compared to the controls, which was restored by probiotics (ZO-1: $F_{(2,15)} = 8.99$, $P = 0.0027$; occludin: $F_{(2,15)} = 8.30$, $P = 0.0037$; claudin-5: $F_{(2,15)} = 20.08$, $P < 0.0001$). Consistently, immunofluorescence staining of the sciatic nerve showed decreased ZO-1 intensities in the PDN group, whereas elevated levels were observed in the probiotics group ($F_{(2,6)} = 11.33$, $P = 0.0092$, Fig. 3I and J). These results indicated that probiotics pretreatment prevented BNB damage in the PDN rats.

Probiotics treatment mitigated intestinal barrier impairment and systemic inflammation

As depicted in the histopathological analysis of H&E-stained colon sections, the control group exhibited a normal colon structure, whereas the PDN group showed inflammatory cell infiltration. Remarkably, in comparison to the PDN group, the probiotics group showed a significant reduction in epithelial impairment and immune infiltration, suggesting a substantial reversal of

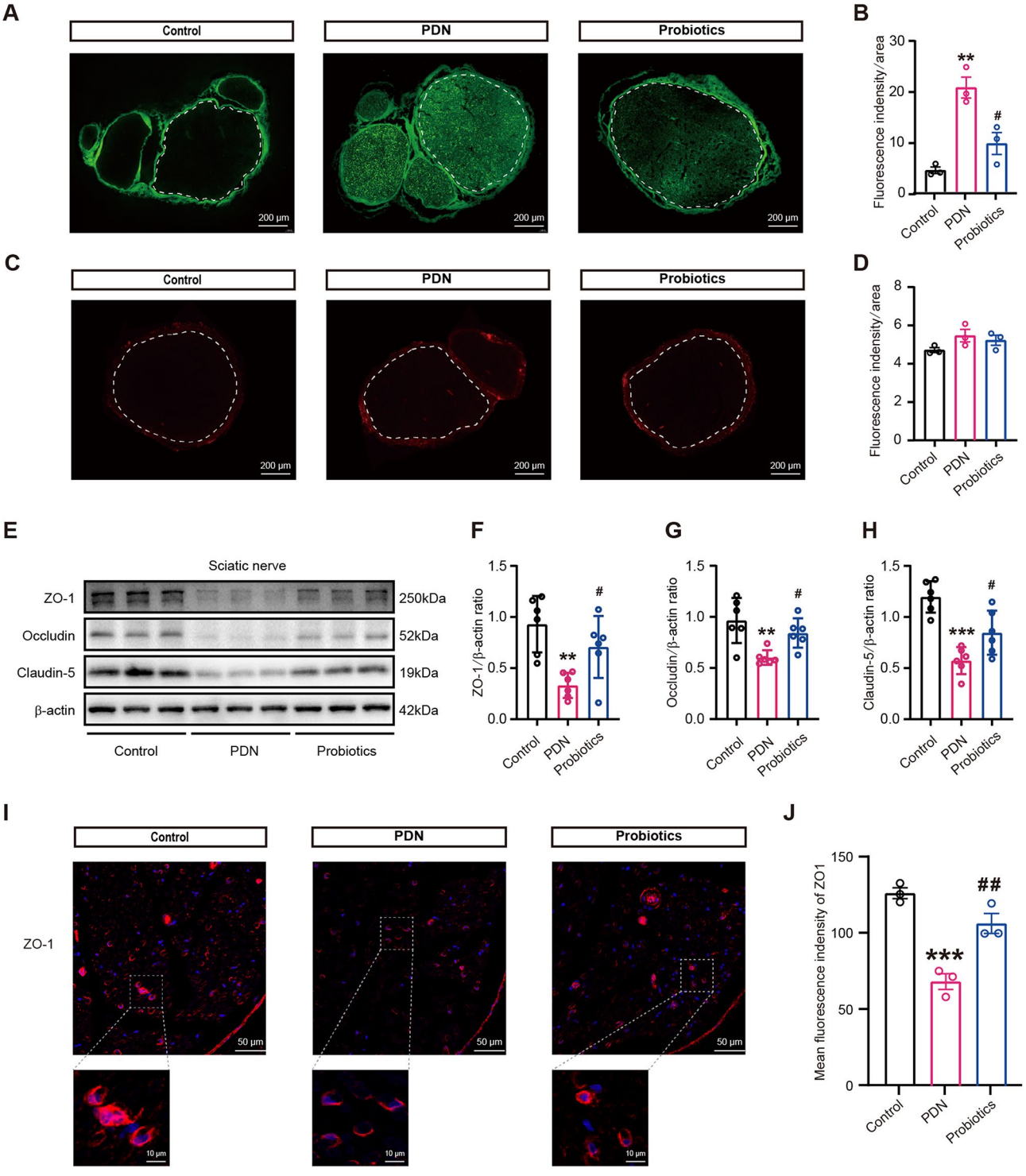

Fig. 3 Probiotics treatment alleviated BNB impairment in PDN rats. (**A**) Representative captures of the in vivo permeability of the BNB to sodium fluorescein (NaFlu) in the sciatic nerve. The fluorescence intensity was measured and standardized based on the region of interest (indicated by the dashed line). Scale bars = 200 μm ($n = 3$). (**B**) The intensity analysis of NaFlu. (**C**) Representative captures of the in vivo permeability of the BNB to Evans Blue albumin (EBA) in the sciatic nerve. The fluorescence intensity was measured and standardized based on the region of interest (indicated by the dashed line). Scale bars = 200 μm ($n = 3$). (**D**) The intensity analysis of EBA. (**E**) Representative Western blot brands of ZO-1, occludin, and claudin-5 in the sciatic nerve ($n = 6$). (**F-H**) Quantification of ZO-1, occludin, and claudin-5 in the sciatic nerve. β-actin was used as the loading control in Western blot analysis. (**I**) Representative captures of immunofluorescence of ZO-1 in the sciatic nerve. The fluorescence intensity was measured and standardized based on the region of interest. Scale bars = 50 μm and 10 μm ($n = 3$). (**J**) The intensity analysis of ZO-1 immunofluorescence staining. Data are presented as mean ± SEM. $^{**}P < 0.01$, $^{***}P < 0.001$ *versus* the control group; $^{\#}P < 0.05$, $^{\#\#}P < 0.01$ *versus* the PDN group, one-way ANOVA with Tukey's multiple comparisons test for (**B**), (**D**), (**F-H**) and (**J**)

colon lesions following 12 weeks of intragastric probiotic administration (Fig. 4A).

The intestinal tight junction plays a crucial role in regulating the permeability of the intestinal barrier. Hence, we assessed the expression levels of tight junction proteins in the colon. As shown in Fig. 4B-E, a marked decrease of the ZO-1, occludin, and claudin-1 expression was noted in the colon of the PDN rats compared to that of the control rats, while probiotics intervention significantly restored the decreased expressions of these proteins in the colon (ZO-1: $F_{(2,15)} = 18.57$, $P < 0.0001$; occludin: $F_{(2,15)} = 12.01$, $P = 0.0008$; claudin-1: $F_{(2,15)} = 20.28$, $P < 0.0001$). Furthermore, lower ZO-1 intensities were decreased in the PDN group compared to the controls, whereas probiotic treatment restored ZO-1 intensities ($F_{(2,6)} = 38.77$, $P = 0.0004$, Fig. 4F and G). These data indicated the beneficial effects of probiotic treatment in restoring the integrity of the intestinal barrier.

Since LPS can diffuse through the leaky gut into the bloodstream [33], and our results showed the alterations in microbiota structure and functional prediction of LPS biosynthesis enrichment, we measured the serum levels of LPS and LPS binding protein (LBP). The PDN group showed significantly higher serum LPS and LBP levels compared to the controls, while probiotics intervention lowered LPS and LBP levels (LPS: $F_{(2,27)} = 32.14$, $P < 0.0001$; LBP: $F_{(2,27)} = 137.2$, $P < 0.0001$, Fig. 4H and I).

Gut bacterial-derived LPS can trigger inflammatory responses and induce systemic inflammation [34]. To assess these, we measured serum levels of IL-6, IL-1β, and TNF-α using ELISA. These cytokines were significantly elevated in the PDN group compared to the controls, whereas pretreatment with probiotics notably prevented these significant increases (IL-6: $F_{(2,27)} = 17.61$, $P < 0.0001$; IL-1β: $F_{(2,27)} = 66.99$, $P < 0.0001$; TNF-α: $F_{(2,27)} = 149.6$, $P < 0.0001$, Fig. 4J-L). These findings suggested that probiotics effectively suppressed systemic inflammation in PDN rats.

Probiotics treatment attenuated neuroinflammation by inhibiting the TLR4/MyD88/NF-κB signaling pathway

We hypothesized that the serum LPS and cytokines may enter into nerves through disrupted BNB and induce neuroinflammation. LPS, a molecular component of the outer membrane of Gram-negative bacteria, binds to its main agonist of TLR4, activating MyD88, and subsequently triggers phosphorylated and degradation of IκBα to release active NF-κB, leading to the production of proinflammatory cytokines [34, 35]. Therefore, we measured the p-IκBα levels and active p65-NF-κB, using an antibody that targets an epitope of the p65 subunit of NF-κB exposed after release from IκBα.

In sciatic nerve samples, the levels of TLR4, MyD88, p-IκBα, and p-p65 proteins were significantly higher in the PDN group compared to the controls, while probiotics treatment notably attenuated these elevations (TLR4: $F_{(2,15)} = 16.00$, $P = 0.0002$; MyD88: $F_{(2,15)} = 6.981$, $P = 0.0072$; p-IκBα: $F_{(2,15)} = 11.52$, $P = 0.0009$; p-p65: $F_{(2,15)} = 14.62$, $P = 0.0003$, Fig. 5A-G). TLR4 signaling activation induces the release of proinflammatory cytokines [35]. Thus, we measured IL-6, IL-1β, and TNF-α levels in the sciatic nerve. In PDN rats, these cytokines increased compared to the control group, whereas pretreatment with probiotics alleviated their elevation (IL-6: $F_{(2,27)} = 20.7$, $P = 0.2490$; IL-1β: $F_{(2,27)} = 38.12$, $P = 0.1270$; TNF-α: $F_{(2,27)} = 14.62$, $P < 0.0001$, Fig. 5H-J).

To assess the relationship between neuroinflammation and pain phenotypes, we conducted correlation analyses of TLR4 signaling-related molecules in the sciatic nerve with both pain behaviors and metrics reflecting neuronal excitability. The increased levels of TLR4, MyD88, p-IκBα, p-p65, IL-6, IL-1β, and TNF-α, indicating TLR4 signaling activation and cytokine release in the sciatic nerve, were correlated with decreased PWT and PWL (representing reduced pain threshold), and neuronal hypersensitivity (including the reductions in the ISI, AHP 80% duration, AP amplitude, AHP amplitude, and TP) (Fig. 5K). In summary, TLR4/MyD88/NF-κB pathway activation by bacterial LPS may induce neuroinflammation and pain in PDN rats. Probiotic treatment alleviates neuroinflammation by suppressing this signaling pathway.

Discussion

In the present study, we demonstrated that PDN rats exhibited pain, nerve injury, and disruptions in gut microbiota composition and function, all of which were mitigated by supplementation with probiotics. Probiotic administration effectively attenuated intestinal barrier disruption and systemic inflammation by reshaping the gut microbiota, ultimately alleviating BNB impairment and neuroinflammation. Further experiments indicated that probiotics supplementation alleviated peripheral inflammation through suppression of TLR4/MyD88/NF-κB signaling. In summary, our work shed light on the therapeutic potential of probiotics for PDN by modulating the microbiota-gut-nerve system axis.

The gut microbiota plays an important role in maintaining host health [6]. Recent studies suggest that alterations in the gut microbiota associated with PDN in patients and may even be a causal factor in its development [36, 37]. In animal models of type 1 diabetes (T1D), gut dysbiosis has been linked to the onset and progression of PDN [38]. However, the relationship between the gut microbiota and PDN in T2D is still scanty. Considering that T2D accounts for over 90% of diabetes cases [39], we utilized a combination of HFD and low-dose STZ injection to mimic T2D conditions, and the changes in

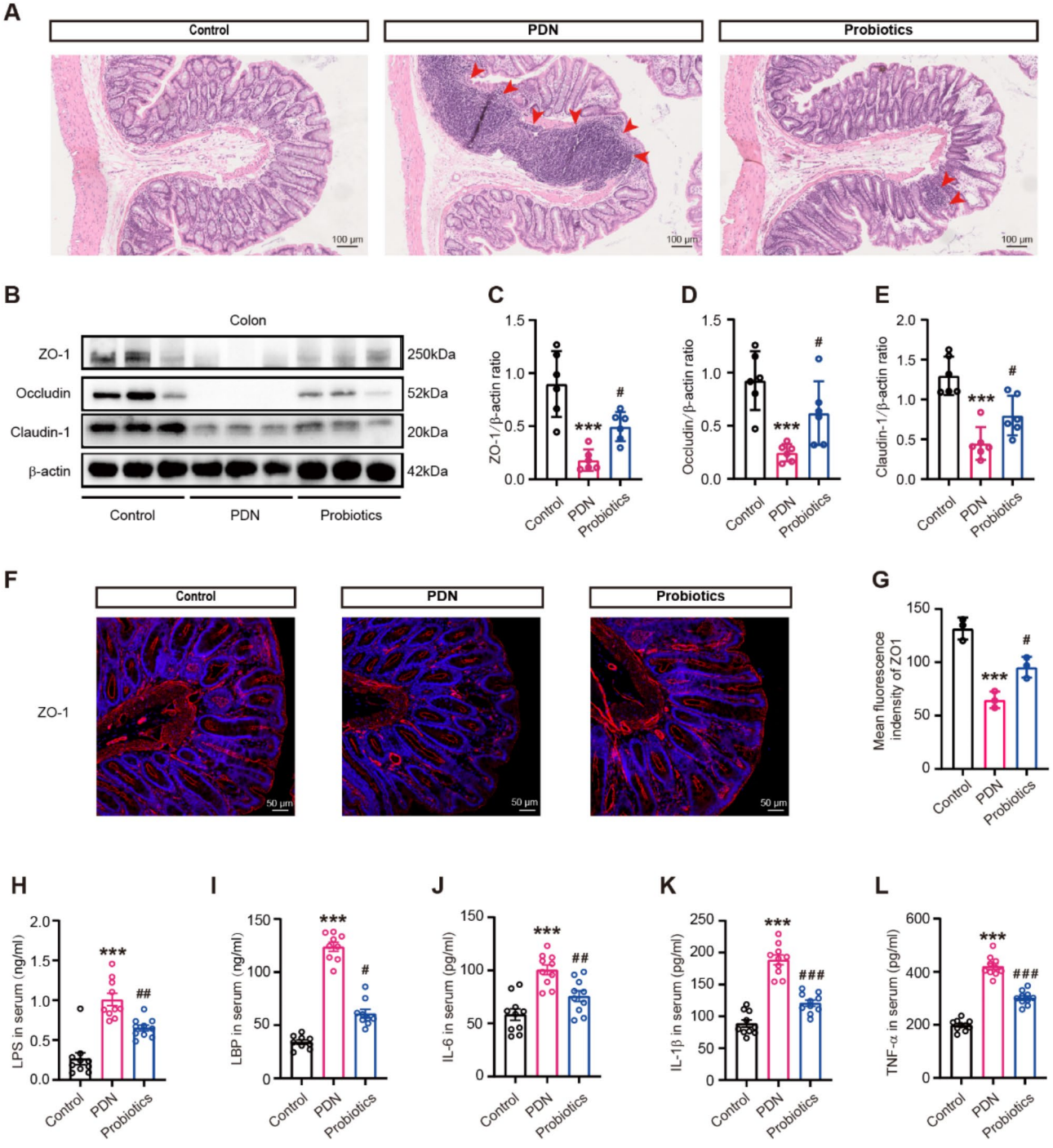

Fig. 4 Probiotics treatment mitigated intestinal barrier impairment and systemic inflammation in PDN rats. (**A**) Representative captures of H&E staining of the colon tissue. The red arrows indicate inflammatory cell infiltration. Scale bars = 100 μm. (**B**) Representative Western blot brands of ZO-1, occludin, and claudin-1 in the colon ($n = 6$). (**C-E**) Quantification of ZO-1, occludin, and claudin-1 in the colon. β-actin was used as the loading control in Western blot analysis. (**F**) Representative captures of immunofluorescence of ZO-1 in the colon. Scale bars = 50 μm. (**G**) The intensity analysis of ZO-1 immunofluorescence staining. (**H-L**) Serum levels of LPS, LBP, IL-6, IL-1β, and TNF-α ($n = 10$). Data are presented as mean ± SEM. Data are presented as mean ± SEM. $^{***}P < 0.001$ *versus* the control group; $^{\#}P < 0.05$, $^{\#\#}P < 0.01$, $^{\#\#\#}P < 0.001$ *versus* the PDN group, one-way ANOVA with Tukey's multiple comparisons test for (**C-E**), (**G**) and (**H-L**)

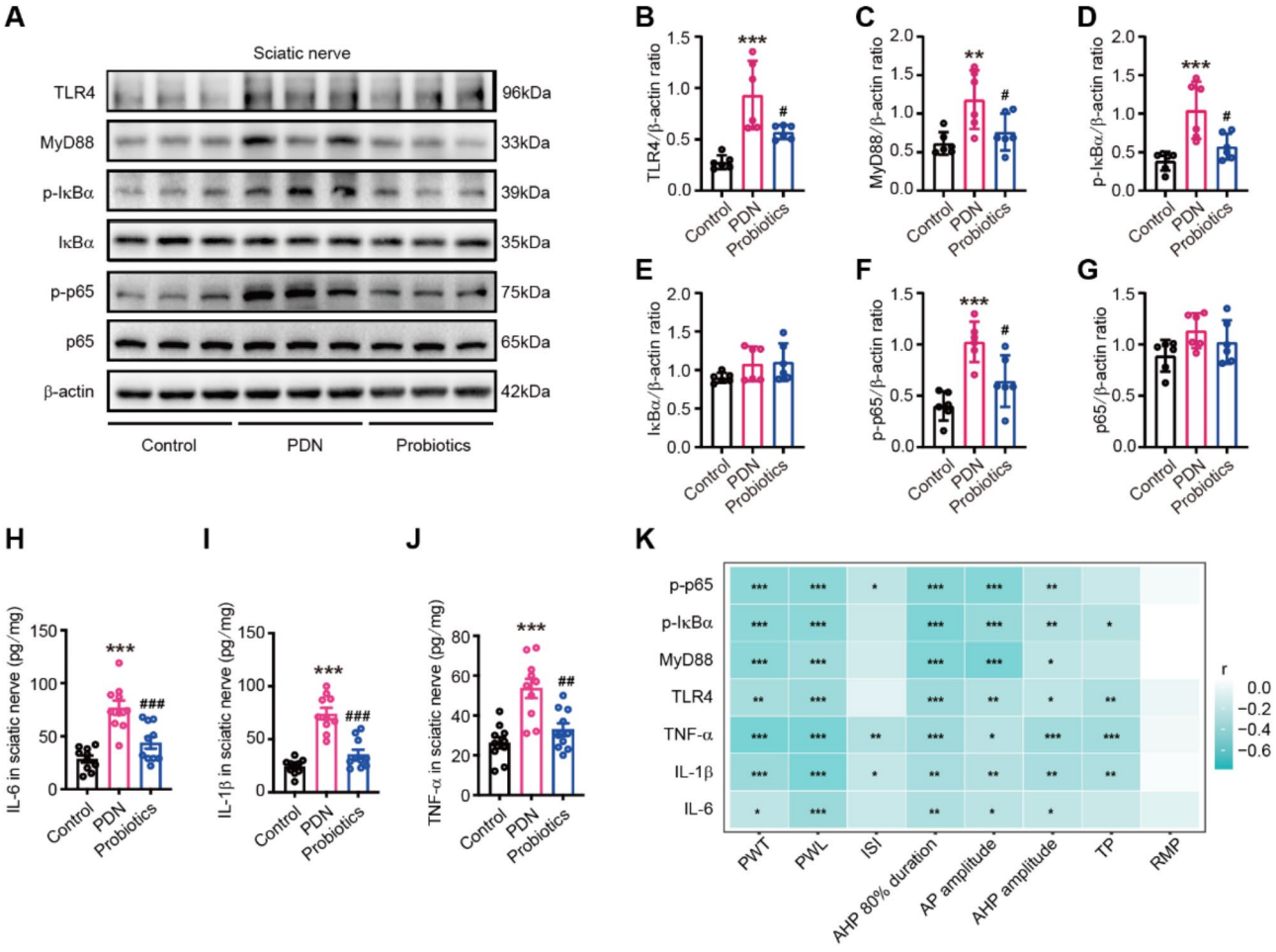

Fig. 5 Probiotics treatment attenuated neuroinflammation by inhibiting the TLR4/MyD88/NF-κB signaling pathway. (**A**) Representative Western blot brands of TLR4, MyD88, p-IκBα, IκBα, p-p65, and p65 in the sciatic nerve ($n=6$). (**B-G**) Quantification of TLR4, MyD88, p-IκBα, IκBα, p-p65, and p65 in the sciatic nerve. (**H-J**) The levels of IL-6, IL-1β, and TNF-α in the sciatic nerve ($n=10$). (**K**) Spearman's correlation heatmap between TLR4 signaling-related molecules and pain-related phenotypes. PWT, paw withdrawal threshold; PWL: Paw withdrawal latency; ISI: Inter-spike interval; AHP: After-hyperpolarization; AP: Action potential; TP: Threshold potential; RMP: Resting membrane potential. Data are presented as mean ± SEM. $^{*}P<0.05$, $^{**}P<0.01$, $^{***}P<0.001$ *versus* the control group; $^{\#}P<0.05$, $^{\#\#}P<0.01$, $^{\#\#\#}P<0.001$ *versus* the PDN group, one-way ANOVA with Tukey's multiple comparisons test for (**B-J**)

gut microbiota in this model were readily detected upon the onset of pain and nerve damage.

Previous studies suggest that gut microbiota play an essential role in T2D and its complications [40, 41], with many reporting an increased F/B ratio and reduced microbial diversity and richness. Our findings of alpha diversity indicated similar overall species richness between groups within a shift in relative taxa abundance within the PDN group, leading to a less even distribution of microbial species, consistent with other T2D models [42, 43]. In the beta diversity analysis, we found that the samples from the PDN rats formed separate clusters from those of the controls, indicating distinct microbiota structures, consistent with previously reported findings [42, 44].

In our study, we found that the gut microbiota composition in the PDN rats was disrupted. At the phylum level, a higher F/B ratio in the PDN rats compared to healthy rats indicated metabolic disorders and obesity. The supplementation of the HFD is responsible for the increase in the F/B ratio, as seen in other animal studies [45, 46]. At the genus level, a significant reduction in *Lactobacillus* abundance was seen in the PDN rats. However, conflicting evidence suggests that diabetes-related dysbiosis may be more species-specific rather than genus-specific [40]. For example, although the *Lactobacillus* genus is associated with T2D, certain species—such as *L. plantarum* [47], *L. reuteri* [48], *L. casei* [49], and *L. gasseri* [50], —showed anti-inflammatory properties and have been used to regulate glucose and lipid metabolism in T2D models. In addition, *Bifidobacterium*, a well-known probiotic and the genus most linked to microbial protection against T2D [51], was also reduced in PDN rats. Along with evidence that multi-strain probiotics are more effective due

to synergistic effects [16, 52], we supplemented the PDN group with a blend containing nine *Lactobacillus* species and five *Bifidobacterium* species as probiotics in subsequent experiments.

Probiotics are live bacteria that, when consumed in adequate amounts, confer benefits to the host by inhibiting harmful bacteria and strengthening the gut barrier [53]. Given the limited effectiveness of pharmaceuticals in managing neuropathic pain and the emerging insights into microbiota-gut-nervous system interactions, there is growing interest in probiotics as a potential adjunctive therapy [54]. Probiotics play a key role in immune regulation by modulating pro- and anti-inflammatory cytokines, which is crucial for alleviating chronic pain [28]. In mice, three weeks of probiotic treatment before nerve injury reduced TNF-α expression in the spinal cord and mitigated pain sensitization [55]. Additionally, probiotic compounds containing multiple *Lactobacillus* and *Bifidobacterium* strains can alleviate pain and inflammation in mice with oxaliplatin-induced neuropathy [56]. In another study using the same probiotic intervention as ours, probiotics significantly reduced alveolar bone loss in ovariectomized rats by regulating gut microbiota and modulating the bone immune response [57]. Moreover, both preclinical and clinical studies indicate that probiotics may alleviate osteoarthritis pain by positively modulating gut microbiota and decreasing the release of metabolites such as LPS into circulation, thus helping to reduce low-grade inflammation [58]. In our study, compound probiotic supplementation attenuated pain by regulating gut microbiota dysbiosis. Further, the KEGG pathway analysis revealed that LPS biosynthesis pathways were enriched in PDN rats, consistent with the elevated plasma LPS levels observed, while LPS reduced after probiotics intervention, indicating that the gut microbiota disturbance was likely the source of the increased LPS. Therefore, targeted probiotic supplementation exerts protective effects by restoring gut microbiota balance and reducing LPS-associated inflammation in PDN.

LPS, the Gram-negative bacteria product, has been identified as an initial factor in the activation of the TLR4 pathway [34]. TLR4 triggers transcription of NF-κB through the MyD88-dependent pathway, which is essential for inflammatory cytokine release [35]. Consistent with the KEGG findings, our study found that both LPS and LBP were increased in serum in PDN rats with the activation of the TLR4/MyD88/NF-κB pathway and the suppression of tight junction proteins in the colon of the PDN group. All of these indicated that gut dysbiosis in this disease model triggered TLR4/MyD88/NF-κB pathway activation and damaged intestinal integrity and at the same time LPS release into circulation, which boosted the release of proinflammatory factors into the bloodstream, thereby causing systemic inflammation and neuroinflammation and BNB damage towards PDN development.

SCFAs, primarily acetate, propionate, and butyrate, serve as energy sources for the colonic epithelium and engage host signaling pathways to regulate inflammation [59]. Among them, butyrate exerts the most significant physiological effects and offers various health benefits, including pain relief in models of obesity [60] and nerve injury-induced pain models [61]. However, in our study, butyrate levels showed no significant difference between the PDN model and control group, only propionate levels were markedly higher in the PDN group. The effects of propionate remain controversial [62]. Some studies suggest beneficial outcomes; for example, increasing colonic propionate in overweight adults may help prevent weight gain [63]. In vitro, propionate also exhibits neuroprotective and neuroregenerative effects on Schwann cells and neurons from the dorsal root ganglia [64]. However, other evidence points to potential drawbacks. In both human and animal studies, propionate has been linked to insulin resistance and compensatory hyperinsulinemia, which over time may promote adiposity and metabolic disorders [65]. Furthermore, in mice with neuropathic pain, SCFAs, including propionate, contribute to pain development by activating microglia and promoting a pro-inflammatory phenotype [66]. Therefore, its potential role as a "metabolic disruptor" and its association with pain progression may be not excluded.

Our study is not without limitations; for example, male rats were used in our study and potentially missed important findings due to sex differences in the microbiota, a focus on LPS-related mechanisms due to LPS biosynthesis enrichment in KEGG analysis which lacks further metabolomic assessments to elucidate microbial metabolic pathways, and the inherent uncertainty of animal models accurately representing human disease.

Conclusion

This study highlights the crucial role of gut microbiota in PDN pathogenesis. Mechanistic investigations reveal that probiotics supplementation with *Lactobacillus* and *Bifidobacterium* strengthened both the intestinal and blood-nerve barriers, thereby suppressing the TLR4/MyD88/NF-κB inflammatory signaling, ultimately reducing nerve damage and alleviating pain. These findings suggest that targeting the microbiota-gut-nerve axis through probiotic supplements may offer a promising therapeutic strategy for PDN.

Abbreviations

T2D	Type 2 diabetes
PDN	Painful diabetic neuropathy
LPS	Lipopolysaccharide
BBB	Blood-brain barrier
BNB	Blood-nerve barrier
FMT	Fecal microbiota transplantation

HFD	High-fat diet
STZ	Streptozotocin
IPGTT	Intraperitoneal glucose tolerance test
PBS	Phosphate-buffered saline
CFU	Colony forming units
PWT	Paw withdrawal threshold
PWL	Paw withdrawal latency
SNCV	Sensory nerve conduction velocity
DRG	Dorsal root ganglion
L4	Lumbar 4
L5	Lumbar 5
NaFlu	Sodium fluorescein
PFA	Paraformaldehyde
EBA	Evans blue albumin
TEM	Transmission electron microscopy
ZO-1	Zonula occludens-1
IL-6	Interleukin-6
IL-1β	Interleukin-1β
TNF-α	Tumor necrosis factor-α
LBP	LPS binding protein
PVDF	Polyvinylidene fluoride
MyD88	Myeloid differentiation factor 88
IκB	Inhibitor of κB
NF-κB	Nuclear factor-κB
ASV	Amplicon sequence variants
SEM	Standard error of mean
TLR4	Toll-like receptor 4
LDA	Linear discriminant analysis
F/B ratio	Firmicutes/Bacteroidetes ratio
ABC	ATP-binding cassette
AP	Action potential
ISI	Inter-spike interval
T1D	Type 1 diabetes
ELISA	Enzyme-linked immunosorbent assays
SCFAs	Short chain fatty acids

Supplementary Information

The online version contains supplementary material available at https://doi.org/10.1186/s12974-025-03352-3.

Supplementary Material 1

Author contributions

Min Li, Guo-gang Xing, Daqing Ma, Ye Jiang, and Jing Yang designed the study. Ye Jiang, Jing Yang, Min Wei, Jiayin Shou, Shixiong Shen, Zhuoying Yu, Zixian Zhang, Yanhan Lyu, and Dongsheng Yang performed the experiments for this work. Ye Jiang, Jing Yang, Wei Min, and Jiayin Shou analyzed data in this study. Jie Cai provided resources and lab management. Ye Jiang, Jing Yang, and Min Wei wrote the manuscript. Min Li, Guo-Gang Xing, Daqing Ma, Jinpiao Zhu, Zhigang Liu, and Yongzheng Han revised the manuscript. All authors contributed to the discussion of the study and have approved the final manuscript.

Funding

This work was supported by the National Natural Science Foundation of China, No. 82071411, 82001329, 82371227 and 82171226; Beijing Municipal Natural Science Foundation, No. 7204325 and 7222105.

Data availability

The datasets used and/or analyzed during this study can be further obtained from the corresponding author.

Declarations

Ethics approval and consent to participate

All animal experiments in this study were approved by the Peking University Animal Care and Use Committee (No. LA2023082) and conducted in accordance with the ARRIVE guidelines.

Consent for publication

Not applicable.

Competing interests

The authors declare no competing interests.

Author details

[1]Department of Anesthesiology, Peking University Third Hospital, Beijing, China
[2]Neuroscience Research Institute, Peking University, Beijing, China
[3]Department of Neurobiology, School of Basic Medical Sciences, Peking University Health Science Center, Beijing, China
[4]Key Laboratory for Neuroscience, Ministry of Education of China and National Health Commission of China, Beijing, China
[5]Perioperative and Systems Medicine Laboratory, Department of Anesthesiology, Children's Hospital, Zhejiang University School of Medicine, National Clinical Research Center for Child Health, Hangzhou, China
[6]Division of Anaesthetics, Pain Medicine and Intensive Care, Department of Surgery and Cancer, Faculty of Medicine, Imperial College London, Chelsea & Westminster Hospital, London, UK

Received: 28 October 2024 / Accepted: 20 January 2025
Published online: 02 February 2025

References

1. Sun H, Saeedi P. IDF Diabetes Atlas: Global, regional and country-level diabetes prevalence estimates for 2021 and projections for 2045 [J]. Diabetes Res Clin Pract. 2022;183:109119. https://doi.org/10.1016/j.diabres.2021.109119.
2. Jensen TS, Karlsson P, Gylfadottir SS, et al. Painful and non-painful diabetic neuropathy, diagnostic challenges and implications for future management [J]. Brain. 2021;144(6):1632–45. https://doi.org/10.1093/brain/awab079.
3. Feldman EL, Callaghan BC, Pop-Busui R, et al. Diabetic neuropathy [J]. Nat Rev Dis Primers. 2019;5(1):42. https://doi.org/10.1038/s41572-019-0097-9.
4. Sloan G, Selvarajah D. Pathogenesis, diagnosis and clinical management of diabetic sensorimotor peripheral neuropathy [J]. Nat Rev Endocrinol. 2021;17(7):400–20. https://doi.org/10.1038/s41574-021-00496-z.
5. Sloan G, Shillo P. A new look at painful diabetic neuropathy [J]. Diabetes Res Clin Pract. 2018;144:177–91. https://doi.org/10.1016/j.diabres.2018.08.020.
6. Fan Y, Pedersen O. Gut microbiota in human metabolic health and disease [J]. Nat Rev Microbiol. 2021;19(1):55–71. https://doi.org/10.1038/s41579-020-0433-9.
7. Winter SE, Baumler A J. Gut dysbiosis: ecological causes and causative effects on human disease [J]. Proc Natl Acad Sci U S A. 2023;120(50):e2316579120. https://doi.org/10.1073/pnas.2316579120.
8. Wang Y, Ye X. Characteristics of the intestinal flora in patients with peripheral neuropathy associated with type 2 diabetes [J]. J Int Med Res. 2020;48(9):300060520936806. https://doi.org/10.1177/0300060520936806.
9. Yang J, Yang X, Wu G et al. Gut microbiota modulate distal symmetric polyneuropathy in patients with diabetes [J]. Cell Metab, 2023, 35(9): 1548-62 e7. https://doi.org/10.1016/j.cmet.2023.06.010
10. Mishra SP, Wang B. A mechanism by which gut microbiota elevates permeability and inflammation in obese/diabetic mice and human gut [J]. Gut. 2023;72(10):1848–65. https://doi.org/10.1136/gutjnl-2022-327365.
11. Yang G, Wei J, Liu P, et al. Role of the gut microbiota in type 2 diabetes and related diseases [J]. Metabolism. 2021;117:154712. https://doi.org/10.1016/j.metabol.2021.154712.
12. Tilg H, Zmora N, Adolph TE, et al. The intestinal microbiota fuelling metabolic inflammation [J]. Nat Rev Immunol. 2020;20(1):40–54. https://doi.org/10.1038/s41577-019-0198-4.
13. Bairamian D, Sha S, Rolhion N, et al. Microbiota in neuroinflammation and synaptic dysfunction: a focus on Alzheimer's disease [J]. Mol Neurodegener. 2022;17(1):19. https://doi.org/10.1186/s13024-022-00522-2.
14. Aho VTE, Houser MC, Pereira PAB, et al. Relationships of gut microbiota, short-chain fatty acids, inflammation, and the gut barrier in Parkinson's disease [J]. Mol Neurodegener. 2021;16(1):6. https://doi.org/10.1186/s13024-021-00427-6.
15. Ghezzi L, Cantoni C, Pinget GV, et al. Targeting the gut to treat multiple sclerosis [J]. J Clin Invest. 2021;131(13). https://doi.org/10.1172/JCI143774.

16. Liao CA, Huang CH, Ho HH, et al. A combined supplement of probiotic strains AP-32, bv-77, and CP-9 increased Akkermansia mucinphila and reduced non-esterified fatty acids and Energy Metabolism in HFD-Induced obese rats [J]. Nutrients. 2022;14(3). https://doi.org/10.3390/nu14030527.
17. Wang Y, Dilidaxi D, Wu Y, et al. Composite probiotics alleviate type 2 diabetes by regulating intestinal microbiota and inducing GLP-1 secretion in db/db mice [J]. Biomed Pharmacother. 2020;125:109914. https://doi.org/10.1016/j.biopha.2020.109914.
18. Jeong JJ, Jin YJ, Ganesan R, et al. Multistrain Probiotics Alleviate Diarrhea by modulating Microbiome-Derived metabolites and Serotonin pathway [J]. Probiotics Antimicrob Proteins. 2024. https://doi.org/10.1007/s12602-024-10232-4.
19. Beilharz JE, Kaakoush NO Maniam J, et al. Cafeteria diet and probiotic therapy: cross talk among memory, neuroplasticity, serotonin receptors and gut microbiota in the rat [J]. Mol Psychiatry. 2018;23(2):351–61. https://doi.org/10.1038/mp.2017.38.
20. Yang J, Yu Z, Jiang Y, et al. SIRT3 alleviates painful diabetic neuropathy by mediating the FoxO3a-PINK1-Parkin signaling pathway to activate mitophagy [J]. CNS Neurosci Ther. 2024;30(4):e14703. https://doi.org/10.1111/cns.14703.
21. Yuan ZL, Liu XD, Zhang ZX, et al. Activation of GDNF-ERK-Runx1 signaling contributes to P2X3R gene transcription and bone cancer pain [J]. iScience. 2022;25(9):104936. https://doi.org/10.1016/j.isci.2022.104936.
22. Obrosova IG, Li F, Abatan OI, et al. Role of poly(ADP-ribose) polymerase activation in diabetic neuropathy [J]. Diabetes. 2004;53(3):711–20. https://doi.org/10.2337/diabetes.53.3.711.
23. Moreau N, Mauborgne A, Bourgoin S, et al. Early alterations of hedgehog signaling pathway in vascular endothelial cells after peripheral nerve injury elicit blood-nerve barrier disruption, nerve inflammation, and neuropathic pain development [J]. Pain. 2016;157(4):827–39. https://doi.org/10.1097/j.pain.0000000000000444.
24. Malong L, Napoli I, Casal G et al. Characterization of the structure and control of the blood-nerve barrier identifies avenues for therapeutic delivery [J]. Dev Cell, 2023, 58(3): 174 – 91 e8. https://doi.org/10.1016/j.devcel.2023.01.002
25. Yu ZY, Geng J, Li ZQ, et al. Dexmedetomidine enhances ropivacaine-induced sciatic nerve injury in diabetic rats [J]. Br J Anaesth. 2019;122(1):141–9. https://doi.org/10.1016/j.bja.2018.08.022.
26. Xia T, Liu CS, Hu YN, et al. Coix seed polysaccharides alleviate type 2 diabetes mellitus via gut microbiota-derived short-chain fatty acids activation of IGF1/PI3K/AKT signaling. Food Res Int. 2021;150(Pt A):110717. https://doi.org/10.1016/j.foodres.2021.110717.
27. Chen S, Zhou Y, Chen Y, et al. fastp: an ultra-fast all-in-one FASTQ preprocessor [J]. Bioinformatics. 2018;34(17):i884–90. https://doi.org/10.1093/bioinformatics/bty560.
28. Guo R, Chen LH, Xing C, et al. Pain regulation by gut microbiota: molecular mechanisms and therapeutic potential [J]. Br J Anaesth. 2019;123(5):637–54. https://doi.org/10.1016/j.bja.2019.07.026.
29. Fusco W, Lorenzo MB, Cintoni M, et al. Short-chain fatty-acid-producing Bacteria: Key Components of the human gut microbiota [J]. Nutrients. 2023;15(9). https://doi.org/10.3390/nu15092211.
30. Ikeda T, Nishida A, Yamano M, et al. Short-chain fatty acid receptors and gut microbiota as therapeutic targets in metabolic, immune, and neurological diseases [J]. Pharmacol Ther. 2022;239:108273. https://doi.org/10.1016/j.pharmthera.2022.108273.
31. Ubogu EE. Biology of the human blood-nerve barrier in health and disease [J]. Exp Neurol. 2020;328:113272. https://doi.org/10.1016/j.expneurol.2020.113272.
32. Ouyang X, Dong C. Ubogu EE. In situ molecular characterization of endoneurial microvessels that form the blood-nerve barrier in normal human adult peripheral nerves [J]. J Peripher Nerv Syst. 2019;24(2):195–206. https://doi.org/10.1111/jns.12326.
33. Cani PD, Amar J, Iglesias MA, et al. Metabolic endotoxemia initiates obesity and insulin resistance [J]. Diabetes. 2007;56(7):1761–72. https://doi.org/10.2337/db06-1491.
34. Park BS, Lee JO. Recognition of lipopolysaccharide pattern by TLR4 complexes [J]. Exp Mol Med. 2013;45(12):e66. https://doi.org/10.1038/emm.2013.97.
35. Kawai T. Signaling to NF-kappaB by toll-like receptors [J]. Trends Mol Med. 2007;13(11):460–9. https://doi.org/10.1016/j.molmed.2007.09.002.
36. Du Y, Neng Q, Li Y, et al. Gastrointestinal autonomic neuropathy exacerbates gut microbiota dysbiosis in adult patients with type 2 diabetes Mellitus [J]. Front Cell Infect Microbiol. 2021;11:804733. https://doi.org/10.3389/fcimb.2021.804733.
37. Xu M, Hao J, Qi Y, et al. Causal effects of gut microbiota on diabetic neuropathy: a two-sample mendelian randomization study [J]. Front Endocrinol (Lausanne). 2024;15:1388927. https://doi.org/10.3389/fendo.2024.1388927.
38. Ma P, Mo R, Liao H, et al. Gut microbiota depletion by antibiotics ameliorates somatic neuropathic pain induced by nerve injury, chemotherapy, and diabetes in mice [J]. J Neuroinflammation. 2022;19(1):169. https://doi.org/10.1186/s12974-022-02523-w.
39. Collaboration N C D R F. Worldwide trends in diabetes since 1980: a pooled analysis of 751 population-based studies with 4.4 million participants [J]. Lancet. 2016;387(10027):1513–30. https://doi.org/10.1016/S0140-6736(16)00618-8.
40. Crudele L, Gadaleta RM, Cariello M, et al. Gut microbiota in the pathogenesis and therapeutic approaches of diabetes [J]. EBioMedicine. 2023;97:104821. https://doi.org/10.1016/j.ebiom.2023.104821.
41. Iatcu CO, Steen A. Gut microbiota and complications of Type-2 diabetes [J]. Nutrients. 2021;14(1). https://doi.org/10.3390/nu14010166.
42. Huang W, Lin Z, Sun A, et al. The role of gut microbiota in diabetic peripheral neuropathy rats with cognitive dysfunction [J]. Front Microbiol. 2023;14:1156591. https://doi.org/10.3389/fmicb.2023.1156591.
43. Liu D, Zhang S, Li S, et al. Indoleacrylic acid produced by Parabacteroides distasonis alleviates type 2 diabetes via activation of AhR to repair intestinal barrier [J]. BMC Biol. 2023;21(1):90. https://doi.org/10.1186/s12915-023-01578-2.
44. Zhang L, Zhang T, Sun J, et al. Calorie restriction ameliorates hyperglycemia, modulates the disordered gut microbiota, and mitigates metabolic endotoxemia and inflammation in type 2 diabetic rats [J]. J Endocrinol Invest. 2023;46(4):699–711. https://doi.org/10.1007/s40618-022-01914-3.
45. Liu Z, Zhou X, Wang W, et al. Lactobacillus paracasei 24 attenuates lipid Accumulation in High-Fat Diet-Induced obese mice by regulating the gut microbiota [J]. J Agric Food Chem. 2022;70(15):4631–43. https://doi.org/10.1021/acs.jafc.1c07884.
46. Gao X, Zhang H, Li K, et al. Sandalwood seed oil improves insulin sensitivity in high-fat/high-sucrose diet-fed rats associated with altered intestinal microbiota and its metabolites [J]. Food Funct. 2021;12(20):9739–49. https://doi.org/10.1039/d1fo02239c.
47. Lee YS, Lee D, Park GS, et al. Lactobacillus plantarum HAC01 ameliorates type 2 diabetes in high-fat diet and streptozotocin-induced diabetic mice in association with modulating the gut microbiota [J]. Food Funct. 2021;12(14):6363–73. https://doi.org/10.1039/d1fo00698c.
48. Fak F, Backhed F. Lactobacillus reuteri prevents diet-induced obesity, but not atherosclerosis, in a strain dependent fashion in Apoe-/- mice [J]. PLoS ONE. 2012;7(10):e46837. https://doi.org/10.1371/journal.pone.0046837.
49. Chen P, Zhang Q, Dang H, et al. Antidiabetic effect of Lactobacillus casei CCFM0412 on mice with type 2 diabetes induced by a high-fat diet and streptozotocin [J]. Nutrition. 2014;30(9):1061–8. https://doi.org/10.1016/j.nut.2014.03.022.
50. Yun SI, Park HO, Kang JH. Effect of Lactobacillus gasseri BNR17 on blood glucose levels and body weight in a mouse model of type 2 diabetes [J]. J Appl Microbiol. 2009;107(5):1681–6. https://doi.org/10.1111/j.1365-2672.2009.04350.x.
51. Gurung M, Li Z, You H et al. Role of gut microbiota in type 2 diabetes pathophysiology [J]. EBioMedicine, 2020, 51: 102590. https://doi.org/10.1016/j.ebiom.2019.11.051
52. Timmerman HM, Koning CJ, Mulder L, et al. Monostrain, multistrain and multispecies probiotics–A comparison of functionality and efficacy [J]. Int J Food Microbiol. 2004;96(3):219–33. https://doi.org/10.1016/j.ijfoodmicro.2004.05.012.
53. Plaza-Diaz J, Ruiz-Ojeda FJ, Gil-Campos M, et al. Mechanisms of action of probiotics [J]. Adv Nutr. 2019;10(suppl1):S49–66. https://doi.org/10.1093/advances/nmy063.
54. Lin B, Wang Y, Zhang P, et al. Gut microbiota regulates neuropathic pain: potential mechanisms and therapeutic strategy [J]. J Headache Pain. 2020;21(1):103. https://doi.org/10.1186/s10194-020-01170-x.
55. Lee J, Lee G, Ko G, et al. Nerve injury-induced gut dysbiosis contributes to spinal cord TNF-alpha expression and nociceptive sensitization [J]. Brain Behav Immun. 2023;110:155–61. https://doi.org/10.1016/j.bbi.2023.03.005.
56. Cuozzo M, Castelli V, Avagliano C, et al. Effects of chronic oral probiotic treatment in Paclitaxel-Induced Neuropathic Pain [J]. Biomedicines. 2021;9(4). https://doi.org/10.3390/biomedicines9040346.
57. Jia L, Tu Y, Jia X, et al. Probiotics ameliorate alveolar bone loss by regulating gut microbiota [J]. Cell Prolif. 2021;54(7):e13075. https://doi.org/10.1111/cpr.13075.

58. Rahman SO, Bariguian F, Mobasheri A. The potential role of Probiotics in the management of Osteoarthritis Pain: current status and future prospects [J]. Curr Rheumatol Rep. 2023;25(12):307–26. https://doi.org/10.1007/s11926-023-01108-7.
59. Koh A, de Vadder F, Kovatcheva-Datchary P, et al. From Dietary Fiber to host physiology: short-chain fatty acids as key bacterial metabolites [J]. Cell. 2016;165(6):1332–45. https://doi.org/10.1016/j.cell.2016.05.041.
60. Bonomo RR, Cook TM, Gavini CK, et al. Fecal transplantation and butyrate improve neuropathic pain, modify immune cell profile, and gene expression in the PNS of obese mice [J]. Proc Natl Acad Sci U S A. 2020;117(42):26482–93. https://doi.org/10.1073/pnas.2006065117.
61. Kukkar A, Singh N, Jaggi AS. Attenuation of neuropathic pain by sodium butyrate in an experimental model of chronic constriction injury in rats [J]. J Formos Med Assoc. 2014;113(12):921–8. https://doi.org/10.1016/j.jfma.2013.05.013.
62. Arora, T., Sharma, R., Frostg, G. Propionate. Anti-obesity and satiety enhancing factor?. Appetite. 2011;56(2): 511–5. https://doi.org/10.1016/j.appet.2011.01.016.
63. Chambers ES, Viardot A, Psichas A, et al. Effects of targeted delivery of propionate to the human colon on appetite regulation, body weight maintenance and adiposity in overweight adults [J]. Gut. 2015;64(11):1744–54. https://doi.org/10.1136/gutjnl-2014-307913.
64. Gruter T, Mohamad N, Rilke N, et al. Propionate exerts neuroprotective and neuroregenerative effects in the peripheral nervous system [J]. Proc Natl Acad Sci U S A. 2023;120(4):e2216941120. https://doi.org/10.1073/pnas.2216941120.
65. Tirosh A, Calay ES, Tuncman G, et al. The short-chain fatty acid propionate increases glucagon and FABP4 production, impairing insulin action in mice and humans [J]. Sci Transl Med. 2019;11(489). https://doi.org/10.1126/scitranslmed.aav0120.
66. Zhou F, Wang X. Short-chain fatty acids contribute to neuropathic pain via regulating microglia activation and polarization [J]. Mol Pain. 2021;17:1744806921996520. https://doi.org/10.1177/1744806921996520.

Publisher's note